CLIMATE CHANGE ASSESSMENT: TEMPERATURE TRENDS IN THE VÍR I RESERVOIR'S CATCHMENT

Martin Bednář[*1]

[*]Martin.Bednar2@vut.cz

[1]Brno University of Technology, Faculty of Civil Engineering, Institute of Landscape Water Management, Veveří 331/95, 602 00 Brno

Abstract

Climate change poses a profound challenge, impacting ecosystems, human populations and water resources. Adapting water resources to the evolving hydro-climatological conditions within river basins is paramount. This study assesses the climate change effects in the catchment above the Vír I reservoir, located on the Svratka River in the Czech Republic, Central Europe. To account for the uncertainty of climate change, an ensemble approach was employed. Using insights from 13 global climate models (CMIP6, SSP2-4.5 scenario), temperature variations were analysed. The analysis aims to provide insights into temperature variations within this catchment area, shedding light on the complexities of climate change impacts and their implications for water resource management.

Keywords

Climate change, Vír I reservoir, CMIP6, trend, multi-model ensemble

1 INTRODUCTION

Climate change poses a profound challenge, affecting ecosystems, human populations and vital water resources worldwide [1]. The effects of climate change are observed in Central Europe where the extreme weather and its consequences occur more frequently [2]. Consequently, this change affects the water cycle which leads to a change in the hydrological conditions in the landscape [3]. In response to this challenge, it is essential to adapt water resource management strategies to the evolving hydro-climatological conditions within river basins. Central Europe, specifically the Czech Republic, is no exception to the far-reaching impacts of climate change. In this region, one of the prominent water bodies confronted with the impending shifts in temperatures and climate patterns is the Vír I reservoir, situated on the Svratka River.

In order to address the multifaceted uncertainties related to climate change, an in-depth assessment of the temperature trends was undertaken within the catchment area above the Vír I reservoir. This study employs an ensemble approach, utilizing insights from 13 global climate models (GCMs) under the Coupled Model Intercomparison Project Phase 6 (CMIP6) climatological projection, with a specific focus on the middle-range shared socioeconomic pathway scenario SSP2-4.5. Temperature represents a fundamental climatological variable of interest in this analysis, and it serves as a valuable indicator for understanding climate change impacts. The primary objective is to provide critical insights into the variations in temperature within this catchment area, shedding light on the complexities of climate change effects and their implications for water resource management.

This study encompasses an examination of historical temperature data from 1980 to 2014 as well as modelled data projecting into the future, up to 2100. The analysis of these extensive datasets provides us with the means to examine temperature trends, seeking to understand the patterns of change, their significance, and their potential consequences. As the research in this study spans over distinct temporal windows, the temperature trends will be examined in near-term (2015–2040), mid-term (2041–2070) and long-term (2071–2100) periods. The results of these assessments, which will be delved into further, illustrate how temperature trends can significantly change even within different seasons. The insights derived from this research are essential not only for enhancing our understanding of the ongoing climatic shifts but also for supporting future strategies to adapt and mitigate the impacts of climate change, especially in the context of water resource management in the Czech Republic. As the ever-evolving climate challenges are being grappled with, the data and trends presented in this study are invaluable for our collective efforts to safeguard these vital resources.

In the next phase of the investigation, attention will be turned to hydrological rainfall-runoff modelling, building upon foundations laid by the temperature trends analysis. This expanded analysis will aim to evaluate how climate-induced changes in temperatures impact hydrological processes, particularly in terms of precipitation

and runoff dynamics. By coupling this forthcoming research with temperature trend assessment, a more comprehensive understanding of the Vír I reservoir's robustness in the face of climate change will be achieved.

2 STUDY AREA

The temperature trend assessment is presented on the Vír I reservoir's catchment. The reservoir is situated on the Svratka river in the Czech Republic in Central Europe. This region was selected for many reasons. The Vír I reservoir is one of the main surface water resources in the South Moravian region and its catchment has a long history of climatological measurement. Moreover, some climate change analyses had been conducted on the reservoir regarding its water supply purpose [4], [5]. The catchment area is 366.8 km^2. Fig. 1 shows the study area location with all the meteorological stations within and around the catchment. The temperature data were gathered from only three stations located on each side of the catchment, specifically the Svratouch, Nedvězí and Polička stations because all the other stations only measure precipitation.
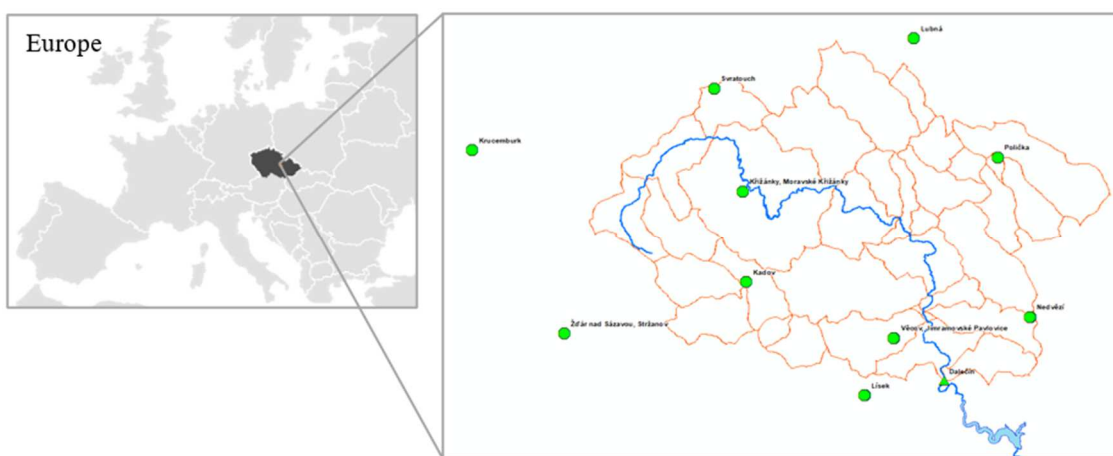

Fig. 1 Study area location with meteorological stations highlighted, Svratka River and Vír I reservoir.

3 METHODS

Data

The daily temperature data were collected from three climatological stations within the study area, specifically the Svratouch, Polička and Nedvězí stations. The data were provided by the Czech Hydrometeorological Institute via their website (https://www.chmi.cz/historicka-data/). The length of observations was set at the range from 1980 to 2014 to match the length of modelled historical data from the GCMs. The modelled historical and predicted temperature data were provided by the Lawrence Livermore National Laboratory via the database containing the World Climate Research Programme data for the CMIP6 (https://esgf-node.llnl.gov/projects/cmip6/). The modelled historical and predicted future data were obtained for a total of 13 GCMs (ACCESS-CM2, ACCESS-ESM1-5, CMCC-ESM2, EC-Earth3, EC-Earth3-Veg-LR, GFDL-ESM4, IITM-ESM, INM-CM4-8, INM-CM5-0, MIROC6, MPI_ESM1-HR, MPI-ESM1-2-LR, NorESM2-MM). Only the data for the "middle-road" climate scenario (SSP2-4.5) were used. The variant label was "r1i1p1f1" for all the selected GCMs.

Spatial downscaling

A generally applied method to extract the station point data from the GCM's output is to assign the variable a value represented by the grid cell in which the station is located [6]. This approach is adequate in the case of high-resolution grids which are mostly seen in regional climate models because the grid cell size is relatively small. However, the GCM outputs used in this study are evaluated on a low-resolution grid, thus, the distance difference between two consecutive cells is large. Due to this, the cell value assignment mentioned above is not a valid approach because two relatively close stations can get assigned a different value, just because they were located on the border of two grid cells. Therefore, spatial interpolation of the point data from the GCM outputs is conducted

using the inverse distance weighting (IDW) method which averages point data based on the distance between the station and four closest grid cells. This method is proven to be easy yet effective in comparison to other existing approaches [7], [8].

The first step of the IDW is determining the distance from the point (station) in which the interpolated data are desired to the four nearest grid cells. However, since the GCM outputs are not in a simple rectangular projection but account for the Earth's curvature, spherical coordinates had to be used in the distance evaluation. The distance D is calculated using the cosine equation [9] as follows (Eq. 1):

$$D = \cos^{-1}[\cos a_1 \cos a_2 \cdot (\cos b_1 \cos b_2 + \sin b_1 \sin b_2) + \sin a_1 \sin a_2] \tag{1}$$

where $[a_1, b_1]$ and $[a_2, b_2]$ are latitude (a) and longitude (b) for the desired point and grid cell, respectively.

In the next step, the weights for each of the four distances are calculated using Eq. 2. The closer the station is to the grid cell, the higher the weight which is determined by the inverse distance between these two points.

$$W_i = \frac{1}{D_i^p}\left(\sum_{i=1}^{4} \frac{1}{D_i^p}\right)^{-1} \tag{2}$$

where W_i is the weight of i-th grid cell with its distance D_i and p is the power exponent determining the rate of weighting regarding the distances. Commonly, the exponent value is to be set to 1 which was used in this study as well. Finally, the interpolated data in the desired point (station) are evaluated as a sum of weighted data from the four nearest grid cells (Eq. 3).

$$data_{station} = \sum_{i=1}^{4} W_i \cdot data_{cell,i} \tag{3}$$

Bias correction

GCMs' outputs are often not representative of observed values but are systematically biased due to model conceptualisation. This bias has to be corrected [10], [11]. In this study, the linear scaling method was used in combination with the variance scaling method [12]. The method corrects modelled temperature data on a monthly basis using the monthly mean values and the monthly standard deviation values (Eq. 4).

$$T_{cor}^t = \mu(T_{gcm}^m) + \left[\mu(T_{obs}^m) - \mu(T_{gcm}^m)\right] + \frac{\sigma(T_{obs}^m)}{\sigma(T_{gcm}^m)}\left[T_{gcm}^t - \mu(T_{gcm}^m)\right] \tag{4}$$

where T^t is mean daily temperature in timestep t and it is in °C, $\mu(\cdot)$ is mean monthly temperature in month m and it is in °C and $\sigma(\cdot)$ is standard deviation in month m and it is in °C for $m = 1, \ldots, 12$. Subscripts "cor","gcm" and "obs" denote corrected, modelled (by GCM) and observed data, respectively.

Trend analysis

To examine the nature of the temperature trends and the significance level in the study area, the Mann-Kendall (MK) trend test and Sen's slope estimate were employed. The MK trend test is a non-parametric test used to identify a trend in a series. The monotonic trend is determined to be either upward or downward. The MK test is commonly employed to detect monotonic trends in a series of environmental data [13].

The null hypothesis (H_0) shows no trend in the series and the data which come from an independent population are identically distributed. The alternative hypothesis (H_a) indicates that the data follow a monotonic trend. Firstly, the MK test statistic (S) is calculated as follows (Eq. 5 and 6):

$$S = \sum_{i=1}^{n-1}\sum_{j=i+1}^{n} sgn(x_j - x_i) \tag{5}$$

where

$$sgn(x_j - x_i) = \begin{cases} 1 & for \quad (x_j - x_i) > 0 \\ 0 & for \quad (x_j - x_i) = 0 \\ -1 & for \quad (x_j - x_i) < 0 \end{cases} \tag{6}$$

If S > 0, then the later observations in the time series tend to be larger than those that appear earlier in the time series, and it is an indicator of an increasing trend and vice versa (decreasing trend when S < 0). The mean of S equals 0 and the variance of S is given by Eq. (7.

$$\sigma^2 = \frac{1}{18}\left[n(n-1)(2n+5) - \sum_{j=1}^{p} t_j(t_j - 1)(2t_j + 5)\right] \tag{7}$$

where p is the number of the tied groups in the data set and t_j is the number of data points in the j-th tied group. The statistic S is approximately normally distributed, provided that the following Z-transformation is employed (Eq. 8):

$$Z = \begin{cases} \dfrac{S-1}{\sqrt{\sigma^2}} & for \quad S > 0 \\ 0 & for \quad S = 0 \\ \dfrac{S+1}{\sqrt{\sigma^2}} & for \quad S < 0 \end{cases} \tag{8}$$

If the Z value is positive, then the trend is increasing while a negative Z value indicates a decreasing trend. Hamed [14] recommended that there will be a decrease or an increase in the S value when autocorrelation is positive or negative which is underestimated or overestimated by the original variance. Thus, if a trend analysis is conducted for this data using the MK trend test, it will show positive or negative trends when there is no trend. Hence, the modification of the MK test (MK') proposed by [15] was used to remove all (lag-k) serial correlations in the time series of seasonal data. The modified procedure is in correcting the variance of the statistic S using a correction factor (CF) evaluated by the following equation (Eq. 9):

$$CF = 1 + \frac{2}{n(n-1)(n-2)}\sum_{k=1}^{n-1}(n-k)(n-k-1)(n-k-2)r_k^R \tag{9}$$

where r^R_k is lag-ranked serial correlation and n is the total number of observations.

The Sen's slope estimator is another non-parametric test used to identify a trend in a series and what is more, it also shows the magnitude of the trend. The Sen's slope estimate requires at least 10 values in a time series. This test computes both the slope (linear rate of change) and the intercepts according to Sen's method [16]. It can be described as a linear model calculated as follows (Eq. 10):

$$f(x) = Qx + B \tag{10}$$

where Q is the slope and B is the constant intercept. The set of linear slopes is calculated using Eq. 11.

$$Q_i = \frac{X_j - X_k}{j - k} \tag{11}$$

where Q is the slope, X denotes the variable and j,k are indices where $j > k$ for $j= 1, 2, 3, …, N$, where N is the number of data. The slope is estimated for each observation and the corresponding intercept is also the median of all intercepts. The median is computed from the N observation of the slope to estimate the Sen's slope estimator. The positive slope Q_i shows an increasing/upward trend whereas the negative slope Q_i shows a decreasing/downward trend.

4 RESULTS

Firstly, the daily data were aggregated into seasonal averages which were analysed both separately and together in a series. The results for the ensemble of 13 GCMs were graphically tested to see if they can represent a historical period adequately. Fig. 2 depicts the minimum, mean and maximum ensemble temperatures in comparison to the observations for each season separately within the historical period 1980–2014. Fig. 2a shows the ensemble result for a winter season (DJF) where the observed temperatures ranged from –5.7 °C to +1.7 °C. The ensemble minimum and maximum values enveloped the observation although with a wider range (from –9.5 °C to 2.8 °C). The mean ensemble value closely corresponds to the observed values, the mean values do not show the same variance in comparison to the observations. It is worth noting that the variability within the ensemble is provided via each GCM simulation, although these details are not shown in Fig. 2 for clarity. Fig. 2b presents the spring season (MAM) where the observed temperature ranged from 4.1 °C to 9.2 °C. Once again, the ensemble data enveloped the observation within a wider interval (from 1.3 °C to 10.9 °C). This behaviour is also observed in the summer season (JJA; Fig. 2c) and the fall season (SON; Fig. 2d) where the observed and modelled temperature ranges from 14.1 °C to 18.7 °C and from 12.3 °C to 21.4 °C, respectively. Fig. 3 finally represents an aggregation

of all seasons together where the ensemble and observed seasonal mean values immensely align. Notably, an apparent increasing trend in this data can be observed, as highlighted in Fig. 2b, 2c and 3.
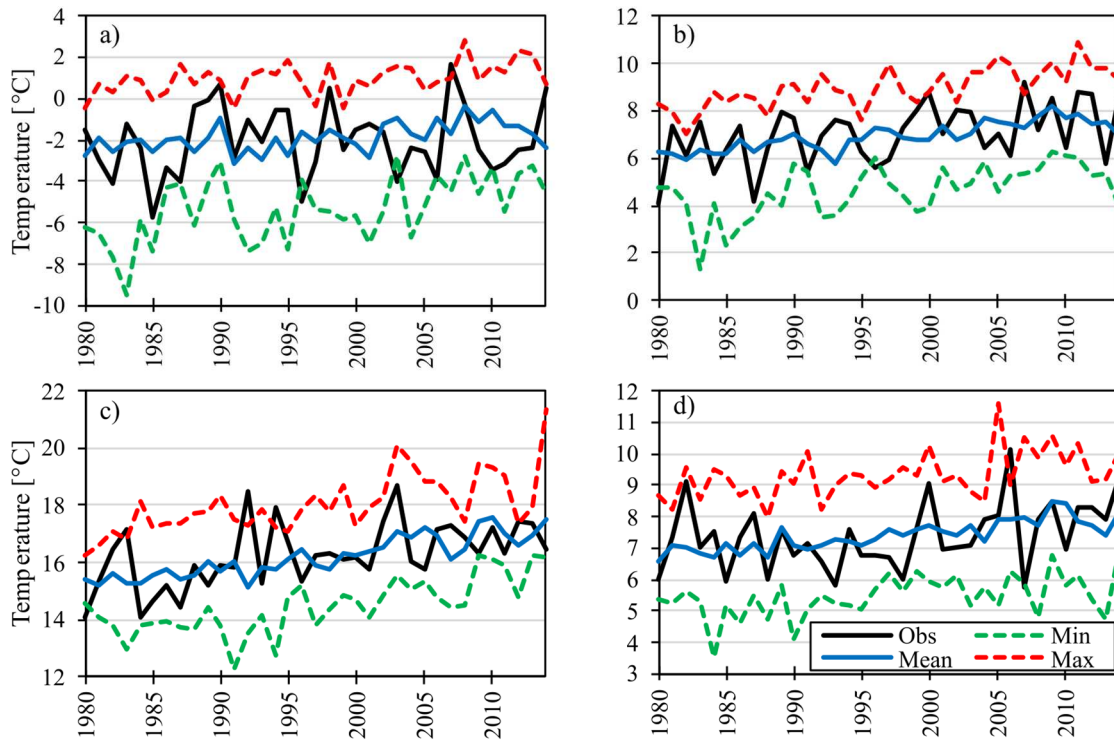

Fig. 2 Mean temperatures during historical period (1980–2014) for: a – winter season (DJF); b – spring season (MAM); c – summer season (JJA); d – fall season (SON); black line – observations; blue line – ensemble mean; green dashed line – ensemble minimum; red dashed line – ensemble maximum.
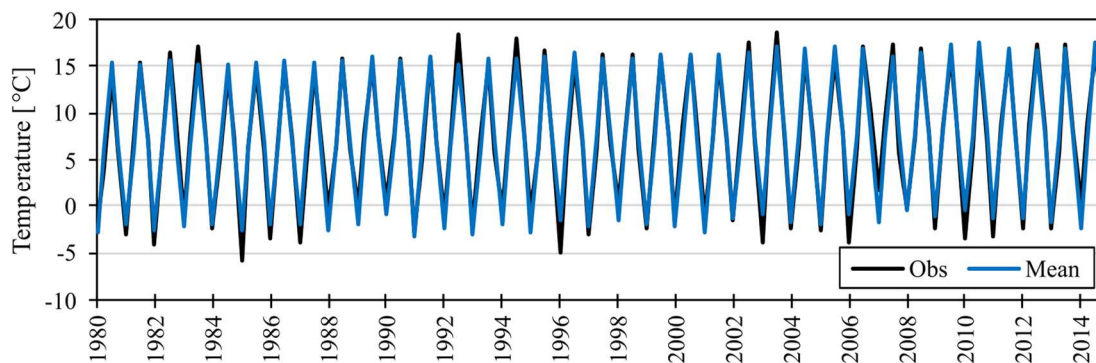

Fig. 3 Seasonal temperature over the entire historical period (1980–2014): black line – observations; blue line – ensemble mean.

Tab. 1 presents the results of the trend analysis for each season separately as well as for all seasons together in the historical period defined as 1980–2014. Having analysed the observed data, an increasing trend is apparent in all seasons during this period . However, there is an exception in the DJF season where the trend is increasing yet statistically insignificant (at a significance level of alpha = 0.05). The ensemble mean, on the other hand, exhibited a statistically significant increasing trend during all seasons as well as across the entire seasonal period. It is worth noting that while the trend significance may not correspond between the observations and modelled data in DJF, the rate of increase (slope) is greatly similar. In fact, the slope is almost identical in all cases in the examined historical period, as presented in Tab. 1. This consistency suggests that the ensemble approach is representative of historical data.

Tab. 1 Trend analysis for each season during the historical period (1980–2014). Observed data and ensemble mean data are presented.

Period	Observed data				Ensemble mean data			
	p-value	Slope	Trend	Significant	p-value	Slope	Trend	Significant
DJF	0.629	0.02	increasing	No	0.001	0.03	increasing	Yes
MAM	0.012	0.05	increasing	Yes	0.000	0.05	increasing	Yes
JJA	0.000	0.06	increasing	Yes	0.000	0.06	increasing	Yes
SON	0.023	0.04	increasing	Yes	0.000	0.04	increasing	Yes
All	0.013	0.15	increasing	Yes	0.001	0.14	increasing	Yes

However, although the ensemble mean is considered representative of the observations, the individual GCMs within the ensemble did not always yield uniform results. Among the ensemble models, there were variations in trend significance. Three out of 13 GCMs showed a statistically significant increasing trend during the DJF season while the results for other nine models aligned with the observed data. In the MAM season, half of the ensemble models showed an insignificant increasing trend while the other half exhibited a significant trend. The trend results for JJA were more consistent, with only one GCM showing an insignificant increasing trend, while the rest displayed significant trends. In the fall season, the entire ensemble displayed an increasing trend, but only five GCMs showed a significant trend. Considering the entire historical period, only three models differed from the results for the observed data, indicating an increasing yet statistically insignificant trend.

While the historical analysis revealed notable variations in trend significance among the individual GCMs within the ensemble, the entire ensemble's overall representation remained consistent. This continuity can be primarily attributed to the ensemble mean's ability to faithfully mirror historical observations. This robust ensemble representation enables exploration of the shared upward trajectory in temperatures across the future periods. These future periods align with the CMIP6 framework, divided into near-term (2015–2040), mid-term (2041– 2070) and long-term (2071–2100) intervals.

Fig. 4a presents both the overall and seasonal mean temperatures during the near-term period, alongside the historical values, to illustrate the observed changes. It is evident that the entire temperature range shifts upwards in all seasons. The smallest change in temperature was observed in the DJF and MAM seasons, with mean temperatures rising by 1.2 °C and 1.0 °C, respectively. The fall season follows with a 1.3 °C increase in mean temperature, while the largest change of 1.4 °C was observed in the JJA. In terms of minimum mean temperature, DJF and MAM remain the seasons with the smallest change, registering increases of 0.9 °C and 0.7 °C, respectively. Subsequently, the summer season showed an increase of 1.1 °C, followed by the fall season with a 1.3 °C increase in minimum mean temperature. Both the MAM and SON seasons exhibit the smallest change in the maximum mean temperature of 1.4 °C. The DJF season recorded a 1.7 °C increase, while the largest change in maximum mean temperature occurred in JJA with a 2.0 °C increase. The overall change in mean temperature, considering all aggregated seasons, is +1.3 °C with a 1.1 °C increase in minimum mean temperature and a 1.6 °C increase in maximum mean temperature. The season showing the most consistent change is the SON, with both minimum and mean temperatures increased by 1.3 °C and the maximum temperature increased by the nearly identical value of 1.4 °C.
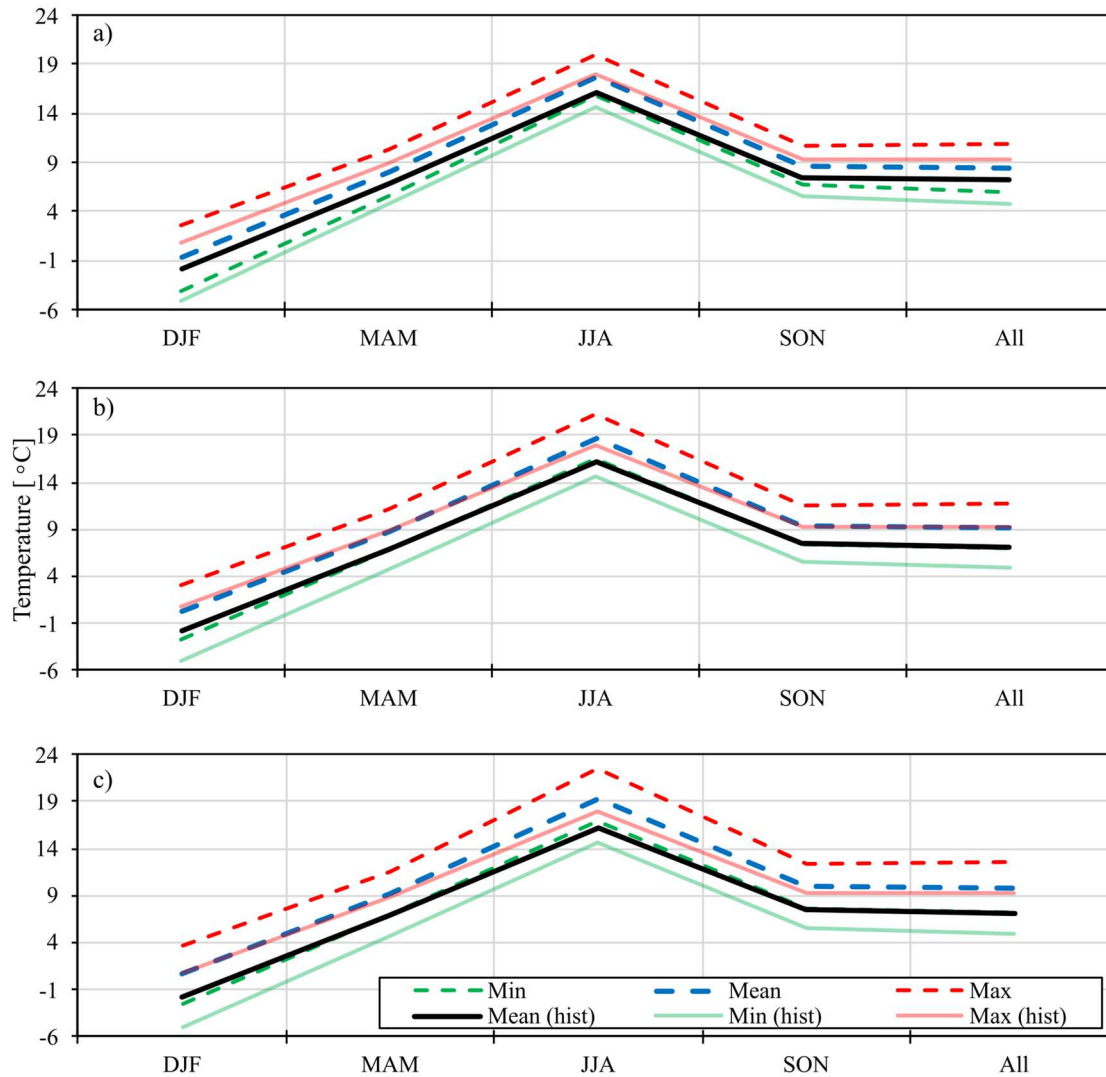
Fig. 4 Seasonal temperature over the future periods: a – near-term period (2015–2040); b – mid-term period (2041–2070); c – long-term period (2071–2100); full lines – ensemble range during historical period; dashed lines – ensemble range during future periods.

Building upon the near-term findings, Fig. 4b illustrates the temperature changes observed during the mid-term period. Once again, a temperature rise can be observed across all seasons. However, the distribution of the temperature change varies compared to the near-term period. The smallest increase of 1.8 °C was observed during the MAM season, closely followed by the SON season with a 1.9 °C increase. In contrast, the DJF season experienced a 2.1 °C increase and the largest change of +2.5 °C, consistent with the previous period, occurred in the JJA. Fig. 4b highlights the substantial upward shift in temperature, with the minimum mean temperature during the period 2041–2070 aligning closely with the historical mean temperature. Additionally, the historical maximum temperature corresponds to the mean temperature within this period.

Lastly, the long-term period, spanning from 2071 to 2100, was analysed to see whether the temperature change trajectory continued over the extended future. The seasonal temperature within this period is depicted in Fig. 4c. It is clear that the temperature rise continued in this period during all seasons. However, the temperature rise was significantly smaller inter-periodically now than it was in between the near-term and mid-term periods. This indicates that the temperature rise is likely to slow down in the second half of the 21st century. Nevertheless, the temperature still rises. The largest increase is observed again in the summer season with a 3.1 °C increase. During both the DJF and SON seasons, the mean temperature rose by 2.6 °C. The MAM season again exhibited the smallest change of +2.3 °C in the mean temperature.

While Fig. 4 visually represented the observed seasonal temperature changes, highlighting the continuous upward trend, the trend was further analysed and evaluated using the Mann-Kendall trend test. The test, accompanied by the Sen's slope values, is presented in the following tables.

Tab. 2 displays the trend analysis results for the near-term period, encompassing the years 2015–2040. During this period, an increasing and statistically significant trend was observed for all seasons. It is worth mentioning that the slope remained unchanged for the DJF, MAM and SON seasons while for the JJA season it was half as much, compared to the historical period. This indicates that the rate of temperature rise during the summer season will be slower in the period 2015–2040, compared to the historical period. Consequently, the overall slope also decreased by 0.02 °C per season, declining from 0.14 °C per season to 0.12 °C per season.

Tab. 2 Trend analysis for each season during the near-term period (2014–2040) using the ensemble mean values.

Period	Ensemble mean (Near-term period)			
	p-value	Slope	Trend	Significant
DJF	0.031	0.03	Increasing	Yes
MAM	0.000	0.05	Increasing	Yes
JJA	0.000	0.03	Increasing	Yes
SON	0.000	0.04	Increasing	Yes
All	0.008	0.12	Increasing	Yes

As depicted in Fig. 4b, the temperature increased during the mid-term period in comparison to the historical period. Tab. 3 shows the results of the trend analysis and the actual differences in the increase of mean temperatures between the near-term and mid-term periods. The increasing trend was evaluated as a statistically significant increasing trend for all seasons. The rates of increase did not significantly change, regarding the near-term period, except for the MAM season where the slope declined from 0.05 °C per season to 0.02 °C per season. Another decline in the slope was observed during the SON season while during the JJA season the slope increased by 0.01 °C per season. The slope for the DJF remained the same at 0.03 °C per season. These changes led to a significant decrease in slope for all periods which declined by 25% from 0.12 °C per season to 0.08 °C per season. The individual differences in the increases in comparison to the previous period correspond to the temperature changes in Fig. 4. The largest differences are observed in both mean and maximum temperatures during the summer season. The DJF season showed the largest differences in minimum temperatures of 1.4°C difference in the increase in temperature. This indicates that during the winter months, the lowest temperatures from the historical period are less likely to occur in the future due to a larger increase compared to mean and maximum temperatures.

Tab. 3 Trend analysis for each season during the min-term period (2041–2070) using the ensemble mean values. The inter-period change is presented as well.

Period	Ensemble mean (Mid-term period)				Change in increase from previous period [°C]		
	p-value	Slope	Trend	Significant	ΔMin	ΔMean	ΔMax
DJF	0.007	0.03	Increasing	Yes	1.4	0.9	0.5
MAM	0.007	0.02	Increasing	Yes	1.2	0.8	0.9
JJA	0.000	0.04	Increasing	Yes	0.8	1.0	1.3
SON	0.000	0.03	Increasing	Yes	0.6	0.7	0.7
All	0.006	0.08	Increasing	Yes	1.0	0.8	0.9

Fig. 4c shows that the temperature increased at a slower rate during the long-term period compared to the mid-term period. This observation is further supported by Tab. 4 where the differences in increases from the previous period are notably smaller in the long-term period, compared to the more significant changes observed between the near-term and mid-term periods. In the mid-term period, minimum mean temperatures increased by an average of 0.6 °C to 1.4 °C compared to the near-term period. However, in the long-term period, this change significantly narrowed down the range to 0.2 °C to 0.4 °C. The rate of change also showed a reduction in mean temperatures, although the reduction was less noticeable in maximum mean temperature.

For the DJF and SON seasons, the temperature change even increased in maximum mean temperatures. This indicates that while the overall temperature increase is slowing down, the likelihood of extreme temperatures occurring in the future remains a concern. Furthermore, the slowing of temperature increase is evident in the slope change as well. The slope remained consistent for the DJF, MAM and SON seasons but halved for the JJA season. A slight slope decline was also recorded in the all-season time series.

Tab. 4 Trend analysis for each season during the long-term period (2071–2100) using the ensemble mean values. The inter-period change is presented as well.

Period	Ensemble mean (Long-term period)				Change in increase from previous period [°C]		
	p-value	Slope	Trend	Significant	ΔMin	ΔMean	ΔMax
DJF	0.005	0.03	Increasing	Yes	0.3	0.5	0.6
MAM	0.011	0.02	Increasing	Yes	0.3	0.5	0.3
JJA	0.019	0.02	Increasing	Yes	0.4	0.7	1.1
SON	0.000	0.03	Increasing	Yes	0.2	0.7	1.0
All	0.003	0.07	Increasing	Yes	0.3	0.6	0.8

5 DISCUSSION

The results demonstrate a statistically significant increasing trend in temperatures throughout all seasons from 2015 to 2100. The final average temperature increase of 2.7 °C during the long-term period (2071–2100) aligns with the projections from the "middle-road" SSP2-4.5 CMIP6 scenario [1]. This increase is compared to the historical period spanning from 1980 to 2014, which already exhibited an upward trend in temperatures, except for the winter season. It is worth noting that Brázdil et al. [17] argued that 30-year normal period defined from 1991 to 2020 was already strongly influenced by recent climate change while the previous normal period from 1961 to 1990 was more stable. This suggests that the temperature increases observed between future periods could be even more pronounced, considering the comparison with a historical period already impacted by climate change. Nevertheless, the overall significance of the increasing trend is in general agreement with the temperature results presented in AR6 (2022).

6 CONCLUSION

The future mean temperature projections were assessed using a multi-model ensemble approach with 13 CMIP GCMs above the Vír I reservoir's catchment. The raw data underwent correction through linear scaling and variance scaling methods, leading to bias-corrected data for evaluation. The comparison of this corrected data with historical observations validated the suitability of the ensemble approach, revealing an acceptable envelope of values that represents the measured data.

Based on these findings, the ensemble was employed to project future mean temperature in the catchment spanning from 2015 to 2100 and divided into near-term (2015–2040), mid-term (2041–2070) and long-term (2071–2100) intervals. Seasonal evaluations showed that the overall increasing trend did not progress uniformly across seasons, with the winter season maintaining a consistent rate of temperature increase throughout the entire period. Despite not exhibiting the highest overall increase, the winter season experienced the most significant rise in minimum mean temperatures, potentially impacting snowmelt patterns and the reservoir´s water management during the winter and spring seasons.

Conversely, the summer season exhibited the largest temperature increases across all three periods, potentially affecting the reservoir´s management during the summer when water demand for irrigation is at its peak. The overall temperature increase is of concern due to its influence on evaporation rates which contribute significantly to the reservoir´s water losses. All in all, the results indicate a steady temperature increase which begins to slow down in the second half of the 21st century, aligning with the projections from the SSP2-4.5 CMIP6 scenario used in this study. Further investigation into these temperature trends and their implications on the reservoir's water management will be conducted in future research as well as rainfall-runoff modelling in the reservoir's catchment.

Acknowledgement

References

[1]   IPCC. *Climate Change 2021: The Physical Science Basis. Contribution of Working Group I to the Sixth Assessment Report of the Intergovernmental Panel on Climate Change* [online]. Cambridge: Cambridge University Press, 2021. [Accessed: 2023-10-24]. Available at:

doi:10.1017/9781009157896

[2] MŽP. Strategie přizpůsobení se změně klimatu v podmínkách ČR [online]. Praha, 2015. [Accessed: 2023-10-24]. Available at: https://www.mzp.cz/C1257458002F0DC7/cz/zmena_klimatu_adaptacni_strategie/$FILE/OEOK-Adaptacni_strategie-20151029.pdf

[3] SKILES, J. W. and Jon D. HANSON. Responses of arid and semiarid watersheds to increasing carbon dioxide and climate change as shown by simulation studies [online]. *Climatic Change*. 1994. 26(4), 377-397. [Accessed: 2023-10-24]. Available at: http://link.springer.com/10.1007/BF01094403

[4] BEDNAR, Martin and Daniel MARTON. Impact of Climate Change on Hydrological and Meteorological Quantities in Watershed Scale [online]. *Proceedings of 22nd International Multidisciplinary Scientific GeoConference SGEM* 2022. STEF92 Technology, 2022, 22(3.2), 91-100 [Accessed: 2023-10-23]. ISSN 1314-2704. Available at: doi:10.5593/sgem2022V/3.2/s12.11.

[5] MARTON, Daniel and Kateřina KNOPPOVÁ. Developing hydrological and reservoir models under deep uncertainty of climate change: robustness of water supply reservoir [online]. *Water Supply*. 2019. 19(8). 2222-2230. [Accessed: 2023-10-24]. Available at: https://iwaponline.com/ws/article/19/8/2222/68927/Developing-hydrological-and-reservoir-models-under.

[6] ZHANG, X.-C. Spatial downscaling of global climate model output for site-specific assessment of crop production and soil erosion [online]. *Agricultural and Forest Meteorology*. 2005.135(1-4), 215-229. [Accessed: 2023-10-24]. Available at: https://linkinghub.elsevier.com/retrieve/pii/S0168192305002534

[7] CHEN, Feng-Wen and Chen-Wuing LIU. Estimation of the spatial rainfall distribution using inverse distance weighting (IDW) in the middle of Taiwan [online]. *Paddy and Water Environment. 2012,* 10(3), 209-222. [Accessed: 2023-10-24]. Available at: http://link.springer.com/10.1007/s10333-012-0319-1

[8] BORGES, Pablo de Amorim, Johannes FRANKE, Yumiko Marina Tanaka DA ANUNCIAÇÃO, Holger WEISS and Christian BERNHOFER. Comparison of spatial interpolation methods for the estimation of precipitation distribution in Distrito Federal, Brazil [online]. *Theoretical and Applied Climatology*. 2016. 123(1-2), 335-348. [Accessed: 2023-10-23]. Available at: http://link.springer.com/10.1007/s00704-014-1359-9

[9] PETERSON, Dave. Distances on Earth1: The Cosine Formula. *The Math Doctors: continuing the mentoring tradition of ask dr. math* [online]. 2021. [Accessed: 2023-10-24]. Available at: https://www.themathdoctors.org/distances-on-earth-1-the-cosine-formula/

[10] CHRISTENSEN, Jens H., Fredrik BOBERG, Ole B. CHRISTENSEN and Philippe LUCAS-PICHER. On the need for bias correction of regional climate change projections of temperature and precipitation [online]. *Geophysical Research Letters*. 2008. 35(20). Available at: http://doi.wiley.com/10.1029/2008GL035694

[11] TEUTSCHBEIN, Claudia and Jan SEIBERT. Bias correction of regional climate model simulations for hydrological climate-change impact studies: Review and evaluation of different methods [online]. *Journal of Hydrology*. 2012. 456-457, 12-29. [Accessed: 2023-10-24]. Available at: https://linkinghub.elsevier.com/retrieve/pii/S0022169412004556

[12] CHEN, Jie, François P. BRISSETTE and Robert LECONTE. Uncertainty of downscaling method in quantifying the impact of climate change on hydrology [online]. *Journal of Hydrology*. 2011. 401(3-4), 190-202. [Accessed: 2023-10-23]. Available at: https://linkinghub.elsevier.com/retrieve/pii/S0022169411001351

[13] ALEMU, Zinabu Assefa and Michael O. DIOHA. Climate change and trend analysis of temperature: the case of Addis Ababa, Ethiopia [online]. *Environmental Systems Research*. 2020. 9(1). [Accessed: 2023-10-23]. Available at: https://environmentalsystemsresearch.springeropen.com/articles/10.1186/s40068-020-00190-5

[14] HAMED, K.H. Enhancing the effectiveness of prewhitening in trend analysis of hydrologic data [online]. *Journal of Hydrology*. 2009. 368(1-4), 143-155. [Accessed: 2023-10-24]. Available at: https://linkinghub.elsevier.com/retrieve/pii/S0022169409000675

[15] HAMED, Khaled H. and A. RAMACHANDRA RAO. A modified Mann-Kendall trend test for autocorrelated data [online]. *Journal of Hydrology*. 1998. 204(1-4), 182-196. [Accessed: 2023-10-24]. Available at: https://linkinghub.elsevier.com/retrieve/pii/S002216949700125X

[16] SEN, Pranab Kumar. Estimates of the Regression Coefficient Based on Kendall's Tau [online]. *Journal of the American Statistical Association*. 1968. 63(324). [Accessed: 2023-10-24]. Available at: https://www.jstor.org/stable/2285891?origin=crossref

[17] BRÁZDIL, Rudolf, Pavel ZAHRADNÍČEK, Petr DOBROVOLNÝ, Jan ŘEHOŘ, Ondřej LHOTKA and Petr ŠTĚPÁNEK. A Comparison of Changes for Two "Normal" Periods [online]. *Atmosphere*. 2022. 13(1). [Accessed: 2023-10-24]. Available at: https://www.mdpi.com/2073-4433/13/1/137